

**Heralded ions via ionization coincidence**

A. J. McCulloch, R. W. Speirs, S. H. Wissenberg, R. P. M. Tielen, B. M. Sparkes, and R. E. Scholten\*  
*School of Physics, The University of Melbourne, Victoria 3010, Australia*

 (Received 29 November 2017; published 23 April 2018)

We demonstrate a method for the deterministic production of single ions by exploiting the correlation between an electron and associated ion following ionization. Coincident detection and feedback in combination with Coulomb-driven particle selection allows for high-fidelity heralding of ions at a high repetition rate. Extension of the scheme beyond time-correlated feedback to position- and momentum-correlated feedback will provide a general and powerful means to optimize the ion beam brightness for the development of next-generation focused ion beam technologies.

DOI: [10.1103/PhysRevA.97.043423](https://doi.org/10.1103/PhysRevA.97.043423)

**I. INTRODUCTION**

High-precision placement of single atoms and ions offers new and exciting prospects for the realization of exotic and powerful devices at the nanoscale, from ordered arrays of dopants in classical semiconductors to single-atom qubits for quantum computing [1–5]. Various mechanisms for the manipulation of single atoms and ions have been demonstrated [6,7], but have been slow or the sources of single ions not deterministic. The precise requirements for a high-performance source of single ions will vary depending on the application, but the ideal source should be capable of generating a high current of single ions that can be focused to an atomic scale, where the presence or absence of an ion is known with high fidelity.

Laser-cooling and -trapping techniques provide promising new approaches to single-ion generation, using both direct and indirect methods. In the direct case, ions themselves are cooled and trapped and can be deterministically outcoupled from the trap [8], which has recently been used to perform ion microscopy [9]. Ion trapping provides excellent control over the ion number and, consequently, these direct sources can create single-ion beams with high fidelity, but the achievable current from such a source is quite limited. Indirectly, ions can be produced from the ionization of trapped atomic samples to create an extremely high-brightness ion source [10–14]. Indirect sources are capable of producing high-current beams, but these sources are not intrinsically deterministic. It has been suggested that a quasideterministic source of single ions could be created from a dipole-blockaded atomic ensemble [15], but this has yet to be realized. Here we present a high-fidelity method for deterministic quasi-single-ion production, based on feedback from detection of the associated electron.

Ionization of cold atoms produces electron-ion pairs, and as both particles are extremely cold, either can be extracted for subsequent use. Cold-atom electron sources (CAESs) have remarkable coherence properties [16–19] and hold promise as a source of electrons for performing ultrafast electron diffraction

(UED) [20] or as an injector for a compact free-electron laser (FEL) [21]. Similarly, cold-ion sources provide high monochromaticity [22–24] and an inherently low transverse emittance [25], suitable for delivering a focal spot size with subnanometer resolution at low beam energy [13]. Recently, a cold-atom ion source was reported to have the highest brightness of any ion source to date [14]. An ultimate goal for these cold-atom sources is to harness both electrons and ions after ionization. Using one species to infer information about the other offers the possibility to correct the ionic trajectory based on the detection of the associated electron. Such a correction could, in principle, improve the ion beam brightness, which is crucial for the development of next-generation focused ion beam (FIB) technologies.

Existing techniques such as coincidence spectroscopy [26] have demonstrated use of correlated electron and ion signals to gain useful information about the ionization event. Cold target recoil ion momentum spectroscopy (COLTRIMS) [27] and the associated magneto-optically trapped-target recoil ion momentum spectroscopy (MOTRIMS) [28] allow precision studies of ionization dynamics and atomic and molecular processes. However, until very recently, no experiments had used real-time feedback to modify the trajectory of one species of a pair of correlated particles based on information gained by direct detection of the other [29].

Here we present the coincident detection of electrons and ions produced from photoionization of a neutral atomic beam. We first investigate the correlation present between the electron and ion pairs and use the detection of an electron to herald ion emission. We then demonstrate low-current heralded quasi-single-ion operation by implementing an active-feedback mechanism. Finally, we detail an extension of the system using Coulomb blockade to realize a high-current heralded quasi-single-ion source, and consider the feasibility of using coincidence detection for increasing ion beam brightness.

**II. MEASUREMENT OF ION HERALDING**

A schematic of the coincidence experiment is shown in Fig. 1. Rubidium effuses from an oven and passes through a

\*scholten@unimelb.edu.au

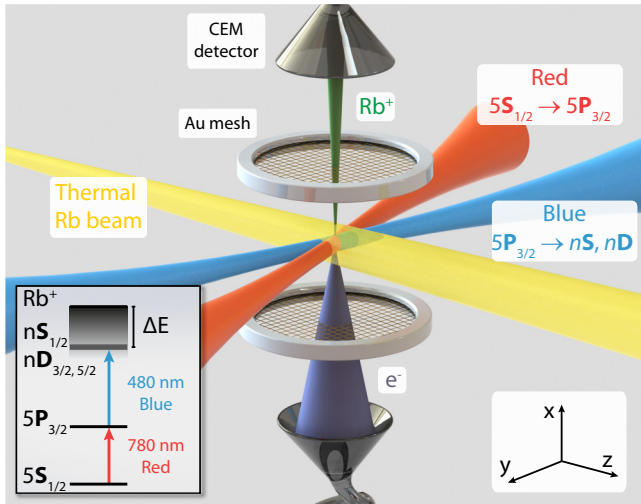


FIG. 1. A schematic of the electron-ion coincidence apparatus. An effusive beam of neutral rubidium enters a region of static electric field between gold mesh electrodes separated by 50 mm. Coupling to Stark states or the ionization continuum is achieved using two-step excitation; red and blue excitation laser beams are near copropagating and directed perpendicular to the electric field. Electrons and ions are detected with channel electron multipliers that are 100 mm from the ionization region. The inset shows the energy-level structure for rubidium.

2-mm-diameter cooled aperture and then propagates 940 mm to the ionization region. Photoionization is performed in a uniform static electric field between 20-mm-diameter gold mesh electrodes separated by 50 mm. Excitation to high-lying Stark states is performed with a two-color process, using a red excitation laser beam to resonantly couple the  $5S_{1/2} F = 3$  and  $5P_{3/2} F = 4$  states, and a blue laser beam coupling the excited  $5P_{3/2}$  state to a Rydberg state or the ionization continuum. The blue laser source is either a narrow-linewidth (linewidth  $< 500$  kHz) continuous laser locked to an optical cavity, or a pulsed laser with 5 ns pulse duration and a linewidth of a few MHz. The red and blue laser beams are near colinear, with a small separation angle to reduce the ionization volume at the focus of the laser beams. The wave vectors of the beams are perpendicular to the electric field, and the polarizations of both beams are linear and can be adjusted independently. Upon ionization, electrons and ions are accelerated towards channel electron multipliers (CEMs) each located 100 mm from the ionization region. The CEM signals are amplified with timing filter amplifiers, and discriminated output signals are connected to a 400-ps-resolution correlation analyzer. Coincidence spectra were generated using a “start-stop” mode of the correlation analyzer, with the detected electron (ion) signals used to start (stop) the coincidence counter.

Ionization occurred in an 800 V/cm field, and outside the ionization region a field of 100 V/cm was used to further accelerate the particles towards the detectors. The blue laser wavelength was tuned to  $\lambda_i = 482.65$  nm, close to the Stark-shifted ionization threshold. The exact state to which excitation and ionization occurred was uncertain because the electric field at the ionization point was not accurately known. Fine

adjustments were made to the blue laser wavelength at a fixed field to optimize the magnitude of the detected electron and ion signals.

The experiment can be run either in continuous or pulsed modes, using the continuous or pulsed ionization laser, respectively. In either mode, the presence of an ion is heralded only by the detection of an electron (and not, for example, by the detection of the laser pulse).

By running in continuous mode, extremely high count rates of heralded ions can be achieved ( $> 1$  MHz). However, to generate heralded single ions, the count rate must be reduced to a very low level (10 kHz), such that the feedback system could faithfully allow passage of at most one ion, as discussed in greater detail in Sec. III.

Running in pulsed mode potentially allows very high rates of heralded single ions to be generated ( $> 100$  kHz) because rather than using active feedback to allow passage of only one ion, the repulsive Coulomb force that exists between groups of more than one ion can be used to filter any heralded events where more than one ion is present, as discussed in Sec. IV. In this way, a high-repetition-rate pulsed laser can be used to generate single ions at the repetition rate of the laser. While no suitable high-repetition-rate ultrafast laser was available for use, the 10 Hz pulsed laser should produce identical results to a high-repetition-rate ultrafast laser, except for the lower maximum ion current commensurate with the reduced laser pulse rate.

A pair of coincidence spectra were obtained to demonstrate that both continuous and pulsed operation modes can reliably produce a heralded ion signal. Figure 2(a) shows a coincidence spectrum for continuous ionization, with a clear peak at a delay time of  $\tau = 1081$  ns. The coincidence signal represents the first step to creating a single-ion source, indicating that it should be possible to herald ions with the detection of electrons. The width of the primary peak was determined by fitting a Gaussian to the coincidence signal, yielding a width of  $\sigma = 5.5$  ns. A very small secondary peak is observed at  $\tau = 1150$  ns, which is believed to result from a second ionization region that is slightly spatially offset from the main region, and is caused by scattered laser light. The height and width of this peak could be dramatically increased by misaligning the ionization laser beam. A near-constant, delay-independent background is measured and can be attributed to the dark counts of the electron and ion detectors in addition to the detection of background particles.

Figure 2(b) is the coincidence spectrum from the same experiment performed using the pulsed ionization laser. The signal-to-noise ratio is much reduced due to the lower count rate commensurate with a large dead time (5 ns pulses at 10 Hz). The location of the peak has shifted slightly to 1058 ns due to a slightly different beam alignment, and the smaller peak width of  $\sigma = 4.3$  ns is because of a smaller overlap region between the red and blue laser beams. The pulsed spectrum does not display a secondary peak as all ionization events occur at one time, over the duration of the pulse (5 ns). This means that if ionization were to occur from multiple regions, the ionization would occur during the same time period (5 ns) and ions from the region with the shortest time of flight (TOF) would always arrive first and stop the coincidence counter, resulting in all other signals being ignored.

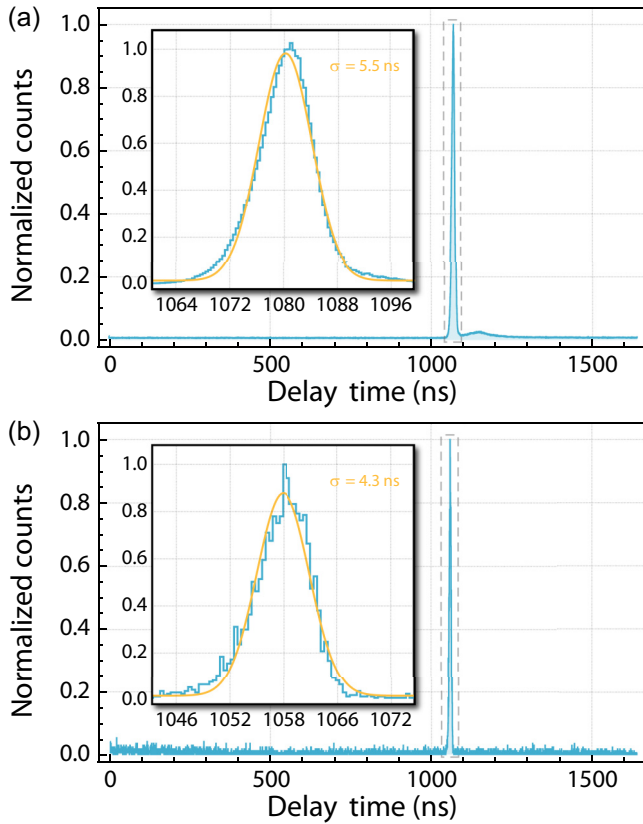


FIG. 2. A coincidence spectrum of electron and ion detection times for ionization using (a) a continuous laser and (b) a pulsed laser. The inset shows the peak region, with a Gaussian fit of the peak data yielding a 5.5 ns coincidence peak width for continuous ionization and 4.3 ns for pulsed ionization.

The width of the coincidence peak limits the precision with which the ion position can be inferred from the detection of an electron at a given time. Peak width can potentially be affected by a variety of factors, such as electron emission angle on photoionization, space-charge interactions in the beam, and the size of the ionization volume. To verify the factors affecting the peak width, particle-tracking simulations were performed. SIMION [30] was used to calculate the electron and ion trajectories and to construct model coincidence spectra. Figure 3(a) shows a schematic for the simulation. Using the same simulation parameters as those found in the experiment

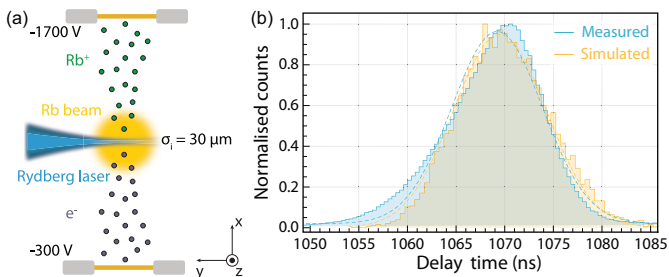


FIG. 3. Simulation of the coincidence spectrum: (a) a schematic of the simulation and (b) the generated coincidence spectrum with the sole fitting parameter of  $\sigma_i = 350 \mu\text{m}$ .

for the simulation, a mean coincidence time of 1070 ns was predicted. This is in agreement with the measured values of 1058 and 1081 ns, with the variation attributable to small differences in ionization beam alignment and hence location of ionization events, and/or field inhomogeneity. The peak width is primarily determined by the size of the ionization volume due to the range of potentials over which atoms are ionized. Space-charge interactions may increase the width, but this effect is negligible for our conditions. If space-charge interactions were present to any significant extent, they would broaden the coincident peak in pulsed experiments to a greater degree than those using the continuous ionization laser due to the higher peak charge density created with the pulsed laser. The peak width in the pulsed spectra is in fact narrower, indicating that space-charge interactions play a negligible role.

The width of the ionization volume  $\sigma_i$  was used as a fitting parameter in the simulations and the best agreement was obtained for  $\sigma_i = 350 \mu\text{m}$  [Fig. 3(b)], much larger than the  $30 \mu\text{m}$  waist of the ionization laser. The larger  $\sigma_i$  suggests that the overlap of the red and blue lasers extends beyond their waists where the beam widths are greater. In particular, angular misalignment of the beams in the  $x$  direction is critical to determining the size of the ionization region due to the small angle between the red and blue lasers resulting in an extended region of overlap in the  $y$  direction. Simulations were also hampered by insufficient knowledge of the effective detector geometry. The point of impact for electron and ion detection was estimated as a plane in the  $x - y$  direction, located at the detector entrance. The location of this plane has a strong influence on the calculated beam width due to the self-focusing of the electron and ion beams. The value of  $\sigma_i$  is therefore only an approximation of the ionization width. To reduce the width of the coincidence signal, a geometry with orthogonal excitation and ionization beams could be implemented, but this was not possible in our apparatus.

The degree of correlation in electron and ion signals is described by the second-order correlation function,

$$g^{(2)}(\tau) = \frac{\langle I_i(t)I_e(t + \tau) \rangle}{\langle I_i(t) \rangle \langle I_e(t) \rangle}, \quad (1)$$

where  $I_{e,i}(t)$  are the intensities (detection rate as a function of time) of the electron and ion signals, and the angled brackets denote the ensemble average. In addition to the start-stop mode, the correlation analyzer could also be used to record the arrival time of all electron and ion detection events over a given period, from which  $g^{(2)}(\tau)$  can be calculated.

Arrival times of all events were recorded under similar conditions to those for the continuous coincidence spectra [Fig. 1(a)], but the field strength in the ionization region was lowered to 340 V/cm and the blue wavelength set to  $\lambda_i = 481.95 \text{ nm}$ . These changes were made to accommodate the installation of a set of electrostatic deflectors between the accelerating mesh and the ion detector, which was used in the feedback presented in Sec. III.

Figure 4 shows the measured second-order correlation function using the arrival times of all detected events recorded over a 600 s period. As expected, there is a peak in  $g^{(2)}(\tau)$  at the time corresponding to the difference in the electron and ion TOF ( $\tau = 7800 \text{ ns}$ ). From the value of  $g^{(2)}$ , it is possible to determine the fraction of total events recorded at one detector

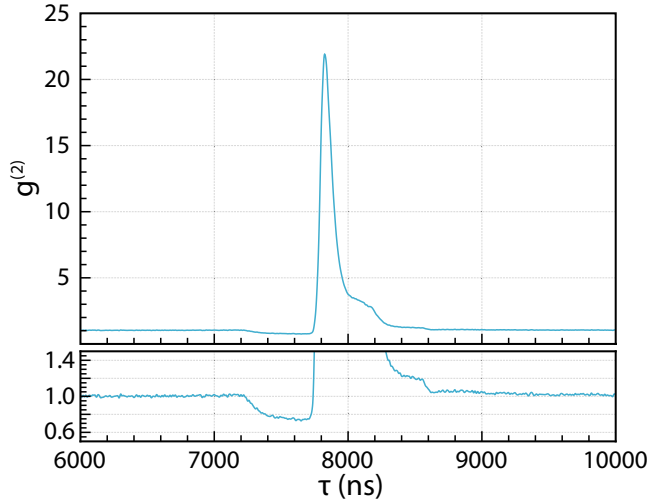


FIG. 4. Measured second-order correlation function for continuous ionization,  $g^{(2)}(\tau)$ . The rate of correlated events can be determined from the sum of all  $g^{(2)}$  bins within the peak. The lower plot shows  $g^{(2)}(\tau)$  around  $g^{(2)} = 1$ , highlighting the small anticorrelation ( $g^{(2)} < 1$ ) immediately preceding the peak.

which had a corresponding detection at the other detector with a time difference  $\tau$ . In this way, the fraction of ions that are successfully heralded can be determined, which gives an indication of the fidelity of the heralding system.

The average rate of correlation  $\gamma_{\text{corr}}$  of recorded events that are correlated with a time delay of exactly  $\tau$  is given by

$$\gamma_{\text{corr}}(\tau) = \frac{-1 + \sqrt{1 + 4\Delta\tau^2\gamma_e\gamma_i(g^{(2)}(\tau) - 1)}}{2\Delta\tau}, \quad (2)$$

where  $\Delta\tau$  is the bin width of  $g^{(2)}(\tau)$ , and  $\gamma_{e,i} \equiv \langle I_{e,i}(t) \rangle$  are the total average rates. Adding together the rates  $\gamma_{\text{corr}}(\tau)$  of all the bins in the peak of  $g^{(2)}(\tau)$  gives the total rate of correlated counts in that range of  $\tau$ .

Given the known total event rates from both detectors and the calculated correlated event rate, the fraction of correlated events recorded at the electron detector was calculated to be 9.1%, and a value of 22.8% was calculated for the ion detector. Put simply, 9.1% of electron detections herald a coming ion detection and 22.8% of ion detections would have heralded an electron detection if they had been detected first. These heralding fractions are for a correlation window between  $\tau = 7740$  and  $8620$  ns, encompassing the peak and the large shoulder of the correlation function. If the window only extends up to  $\tau = 8000$  ns so that only the main peak is included, then the correlated fraction of electron and ion detections drops to 7.2% and 18.2%, respectively.

The width of the correlation function peak is influenced by exactly the same factors as for the coincidence spectra in Fig. 2. The width of the peak in  $g^{(2)}$  is larger than for the peak in the previous coincidence spectra because the installation of the deflector segment increased ion-propagation distance. For a given spread in ion energies, the greater ion TOF results in a larger peak width. The peak is seen to have a secondary bump in the region  $8000 < \tau < 8250$ , which can again be attributed to a secondary ionization region.

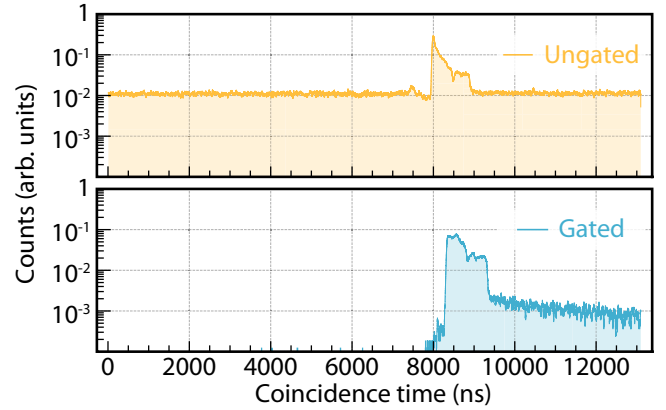


FIG. 5. Coincidence spectra of electron and ion detection times demonstrating feedback. The upper plot shows a coincidence spectrum when no ion gating is implemented and the lower plot shows a coincidence spectrum when ion gating is enacted.

The negative value of  $g^{(2)}$  is due to the finite dead time of the detection system, which in our case is 500 ns, which suppresses detection events in the 500 ns preceding the peak.

The measurements presented above demonstrate that our source generates heralded ions with high fidelity. In the next section, this heralding is used to trigger an active-feedback mechanism allowing the generation of a low current of quasi single ions.

### III. ACTIVE FEEDBACK BASED ON HERALDING

Deflectors between the extraction region and the detection region were added to implement a gating protocol, whereby the deflectors operate to deflect all incident ions away from the detector except when an electron is detected, at which time the deflectors cease deflecting incident ions for a short period. In this way, the only ions that are detected are those which were heralded by the detection of an electron.

To experimentally realize controlled feedback, the detection of an electron was made to trigger a high-voltage switch connected to the electrostatic deflectors, which allowed passage of the associated ion. A delay time of 1100 ns was introduced between the electron detection signal and the start of the deflector switch period to account for the time it takes for the ion to reach the entrance of the deflectors from the position of initial creation. Additionally, an adjustable on-period of the switch was set to 2300 ns, which was just sufficient to allow the ion to traverse the length of the deflectors. The deflector switch had a maximum switching rate of 12 kHz, so to ensure that electrons were generated at less than this rate, the experiment was run at a reduced count rate of approximately 10 kHz. The electron and ion signals were analyzed using the correlation analyzer operating in start-stop mode.

Figure 5 shows coincidence spectra which demonstrate the effect of ion feedback. The upper plot shows a logarithmic-scale coincidence spectrum collected without ion gating, displaying a large coincidence at 7900 ns but with a significant background count at all other times. The background is due to the combination of dark counts on the electron detector, resulting in spurious start signals, and the detection of background

charged particles. The lower plot of Fig. 5 shows a coincidence spectrum collected when gating was enabled, which effectively eliminates the background, leaving only the electrons and ions from ionization events.

For the gated spectrum, there is a reduction in the number of coincident events around the peak by a factor of three, which we attribute to imperfect triggering of the gating system. The delay time at which the peak occurs is at 8551 ns, increased from 8018 ns in the ungated case, which suggests that some deceleration occurs as a result of the switching electrodes. The shape of the peak is also broadened by the switching process, suggesting the deceleration is not uniform in time, but this does not affect the efficacy of heralding.

For the case of the nongated system, the coincident peak accounts for 19.2% of counts within a  $3\sigma$  window, whereas with gating the peak accounts for 89.5%. The counts within the peak provide an approximation of the heralding efficiency; however, because the coincidence analyzer runs until an ion is detected, we cannot discriminate between spurious detection events and nondetection events. Rather, we conclude that for the detection of a given ion, there is a 89.5% (19.2%) probability that the detection event was heralded by the detection of an electron in the gated (ungated) case. These results demonstrate that with a high degree of certainty, the detection of an electron can herald the arrival of an ion.

The correlated feedback method can generate heralded single ions at low count rates. In the next section, we propose a method to achieve very high count rates of heralded single ions.

#### IV. A HIGH-CURRENT QUASI-SINGLE-ION SOURCE

In Sec. II it was shown that the detection of an electron can herald the coming of an ion, and in Sec. III it was shown that this heralding can be used to control an active-feedback mechanism to produce a low-current heralded single-ion source. Here we propose a method to generate a high-current heralded single-ion source, which would use the mutual Coulomb interaction to exclude the passage of ion bunches containing more than a single ion.

By using a high-repetition-rate ultrafast pulsed laser, a high ion current can be achieved even where the average number of ionization events per pulse is set to less than one (which can be easily achieved by making the laser pulse energy very low). Pulses that result in at least one ionization event will be heralded by the detection of an electron, but if two or more ionization events occur in a pulse, the heralding signal will appear identical. The inability to differentiate between the heralding signal coming from single- and multiple-ionization events stems from the fact that the electrons generated in a single pulse will arrive at the detector at almost exactly the same time, which is a consequence of the extremely short duration of the ultrafast laser pulse.

If a small ionization volume is used, the short ionization period will mean that in any pulse where multiple ions are generated, they will be in close proximity and so will experience strong Coulomb repulsion and rapid separation. By placing an aperture in the ion beam path such that off-axis ions are blocked, in general only single ions will be transmitted (Fig. 6).

To test whether such a system is feasible, we have simulated the charged-particle dynamics of the system. Using General Particle Tracer (GPT) [31], we track electrons and ions produced in the system shown in Fig. 1. The simulations were conducted assuming ionization using a  $\sigma_t = 100$  fs laser pulse in an ionization volume characterized by  $\sigma_r = 10 \mu\text{m}$ . The initial temporal and spatial bunch distributions were set to  $\pm 3\sigma_{t,r}$ , respectively. The transverse temperature was 100 mK and the longitudinal beam temperature was 373 K. The electric field strength was set to 2.5 kV/m. The simulated system had a  $50 \mu\text{m}$  aperture located 130 mm from the ionization region and the ion distribution was monitored in the detection plane 150 mm from the ionization region. The aperture was offset from the optical axis 1.9 mm in the direction of the atomic beam propagation to account for the residual momentum of the ions. Figure 6(b)(i)–(iii) shows results after Coulomb-driven expansion for one, two, and three particles generated by the laser pulse, where the images represent the electron distribution in the detector plane. The single-ion case shows minimal beam expansion with a small elongation in the  $y$  direction due to the longitudinal beam temperature. The two-ion case shows only small transmission, peaked at  $+y$  (relative to the single-ion case) as Coulomb interactions act to exacerbate the residual velocity spread from the neutral atomic beam. With three ions, the transmission is more uniform as the Coulomb interactions become more significant, directing the ions in random directions at high velocities. In all cases, 50 000 ions were simulated and transmission rates of 77%, 6%, and 7% were recorded for one, two, and three ions.

The effect of varying each of the simulation parameters was investigated, and it was observed that the longitudinal beam temperature has little effect other than displacing the central beam. Both the ionization time and ionization volume alter the transmission efficiency because they alter the maximum Coulomb forces between ions. Similarly, the extraction field determines the interaction time and hence has a strong effect on the results. The parameters used for the simulation of Fig. 6 were chosen to match those achievable in our experiment. As expected, Coulomb interactions between the electrons were not significant because their small mass results in high velocities for a given energy, and therefore lower interaction times.

The dynamics of femtosecond ionization is complicated [32]. For a 100 fs pulse at 800 nm, the dominant ionization pathway will be resonantly enhanced multiphoton ionization (REMPI) [33]. The power per pulse required such that, on average, a single-ionization event occurs goes as the integrated transition rate  $\Gamma$  for three-photon ionization and is given by

$$\Gamma_{k,g} = 2\pi \hbar (2\pi\alpha F\omega)^3 S(k;g), \quad (3)$$

where  $\alpha$  is the fine-structure constant,  $F$  is the photon flux, and  $\omega$  is the radial frequency of the laser [34]. The ionization strength  $S(k;g)$  is defined by

$$S(k;g) = \frac{\rho}{g_0} \sum_m \int d\Omega_k |\langle \mathbf{k} | \tau^{(3)} | g \rangle|^2, \quad (4)$$

where  $\rho$  is the density of states,  $|g\rangle$  is the ground state,  $g_0$  is the degeneracy of the ground state,  $\langle \mathbf{k} |$  is the ionized electron momentum, and  $\tau^{(3)}$  is the third-order transition operator. The

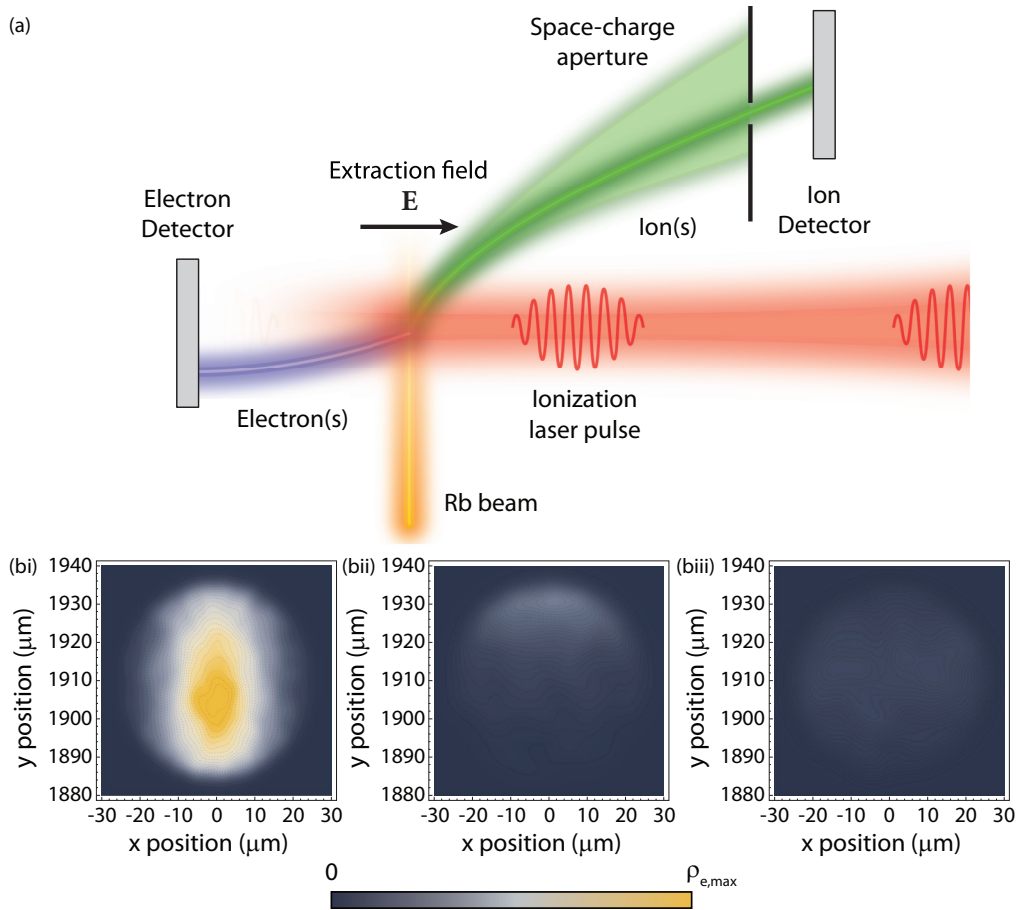


FIG. 6. A deterministic quasi-single-ion source: (a) A schematic of the system. A neutral beam is ionized, the electron is used to herald the ion, and a space-charge aperture is used to quell multi-ionization events. (b) Simulations of the transmission of ions through the aperture given (i) single-, (ii) double-, and (iii) triple-ionization events.

ionization strength describes the coupling from the ground state to an unbound state with momentum  $\mathbf{k}$  via a three-photon transition, the physics of which is encapsulated within  $\tau^{(3)}$ . The values of  $S(k; g)$  have been tabulated and for our parameters of ionization, namely, a  $10\ \mu\text{m}$  spot size and  $1.6\ \text{eV}$  photon energy, to have a single-ionization event on average would require of the order of a few femtoJoules per pulse. In practice, the power could be attenuated until no signal was observed and increased until just a small signal was obtained.

While bunches containing more than one ion rarely end up transmitting even a single ion through the aperture, these bunches still produce a heralding signal. To minimize the number of these false heralding signals, the average number of ions per bunch should be significantly less than one. A low probability of a single-ionization event per pulse could still result in a high count rate of single ions because the repetition rates typical of commercial mode-locked lasers are in the range of  $80\text{--}1000\ \text{MHz}$ . Even with a  $0.1\%$  ionization efficiency (per laser pulse) and a transmission rate of  $77\%$ , count rates of the order of  $60\text{--}720\ \text{kHz}$  would be expected. This is comparable to, or better than, conventional “sweep-mode” single-ion sources, and would represent an improvement in count rate of at least four orders of magnitude compared to other devices capable of nanoscale focusing [9].

Coincident detection of electrons would additionally allow for compressive ghost-imaging ion microscopy. By discounting any counts on the detector which occur outside the coincidence window, a significant gain in the signal-to-noise ratio of ion micrographs is expected. Previously, such schemes have been implemented using optical sources, and a near 100-fold improvement in the signal-to-noise ratio was observed [35].

While the experiments presented here were performed using a thermal beam, cooling the beam would require only the relatively simple addition of a magneto-optical compressor. Such an addition would reduce the ion temperature, which is important for nanoscale focusing of the ion beam, but also improve the ion count rate via increased atomic flux [36,37].

## V. CONCLUSION

We have measured the correlation of electrons and ions produced from an atomic source. The width of the coincidence signal was measured to be  $5\ \text{ns}$  and was primarily determined by the detector geometry. We measured a second-order correlation coefficient  $g^{(2)}(\tau) = 25$  and the correlated fraction of produced electrons and ions to be  $9.1\%$  and  $22.8\%$ , respectively. An

electrostatic gating system enhanced the correlation fraction from 19.2% to 89.5%. An extension of the system to the creation of a deterministic quasi-single-ion source was outlined and simulations suggest strong suppression of ionization events with greater than one ion. All components together provide a platform capable of delivering a high-fidelity, high-count-rate source of single ions which is focusable at the nanoscale. Such a system would be an important first step on the path to creating a “correlation corrector,” a tool for

optimizing ion beam brightness by correcting for the fundamental momentum spread of an ion source.

#### ACKNOWLEDGMENTS

The authors would like to thank Daniel Comparat for useful discussions. This work was supported by the Australian Research Council Discovery Project No. DP170101148 and Linkage Project No. LP150101188.

- 
- [1] T. Shinada, S. Okamoto, T. Kobayashi, and I. Ohdomari, *Nature (London)* **437**, 1128 (2005).
- [2] G. Lansbergen, R. Rahman, C. Wellard, I. Woo, J. Caro, N. Collaert, S. Biesemans, G. Klimeck, L. Hollenberg, and S. Rogge, *Nat. Phys.* **4**, 656 (2008).
- [3] J. A. Van Donkelaar, A. D. Greentree, A. D. Alves, L. M. Jong, L. C. Hollenberg, and D. N. Jamieson, *New J. Phys.* **12**, 065016 (2010).
- [4] P. M. Koenraad and M. E. Flatté, *Nat. Mater.* **10**, 91 (2011).
- [5] M. Fuechsle, J. A. Miwa, S. Mahapatra, H. Ryu, S. Lee, O. Warschkow, L. C. Hollenberg, G. Klimeck, and M. Y. Simmons, *Nat. Nanotechnol.* **7**, 242 (2012).
- [6] D. M. Eigler and E. K. Schweizer, *Nature (London)* **344**, 524 (1990).
- [7] T. Shinada, H. Koyama, C. Hinoshita, K. Imamura, and I. Ohdomari, *Jpn. J. Appl. Phys.* **41**, L287 (2002).
- [8] W. Schnitzler, N. M. Linke, R. Fickler, J. Meijer, F. Schmidt-Kaler, and K. Singer, *Phys. Rev. Lett.* **102**, 070501 (2009).
- [9] G. Jacob, K. Groot-Berning, S. Wolf, S. Ulm, L. Couturier, S. T. Dawkins, U. G. Poschinger, F. Schmidt-Kaler, and K. Singer, *Phys. Rev. Lett.* **117**, 043001 (2016).
- [10] J. L. Hanssen, S. B. Hill, J. Orloff, and J. J. McClelland, *Nano Lett.* **8**, 2844 (2008).
- [11] M. P. Reijnders, N. Debernardi, S. B. van der Geer, P. H. A. Mutsaers, E. J. D. Vredenburg, and O. J. Luiten, *Phys. Rev. Lett.* **105**, 034802 (2010).
- [12] D. Murphy, R. W. Speirs, D. V. Sheludko, C. T. Putkunz, A. McCulloch, B. M. Sparkes, and R. E. Scholten, *Nat. Commun.* **5**, 4489 (2014).
- [13] M. Viteau, M. Reveillard, L. Kime, B. Rasser, P. Sudraud, Y. Bruneau, G. Khalili, P. Pillet, D. Comparat, I. Guerri *et al.*, *Ultramicroscopy* **164**, 70 (2016).
- [14] A. V. Steele, A. Schwarzkopf, J. J. McClelland, and B. Knuffman, *Nano Futures* **1**, 015005 (2017).
- [15] C. Ates, I. Lesanovsky, C. S. Adams, and K. J. Weatherill, *Phys. Rev. Lett.* **110**, 213003 (2013).
- [16] A. McCulloch, D. Sheludko, S. Saliba, S. Bell, M. Junker, K. Nugent, and R. Scholten, *Nat. Phys.* **7**, 785 (2011).
- [17] A. McCulloch, D. Sheludko, M. Junker, and R. Scholten, *Nat. Commun.* **4**, 1692 (2013).
- [18] W. Engelen, M. van der Heijden, D. Bakker, E. Vredenburg, and O. Luiten, *Nat. Commun.* **4**, 1693 (2013).
- [19] O. Fedchenko, S. Chernov, A. McCulloch, M. Vielle-Grosjean, D. Comparat, and G. Schönhense, *Appl. Phys. Lett.* **111**, 021104 (2017).
- [20] G. Taban, M. Reijnders, B. Fleskens, S. van der Geer, O. Luiten, and E. Vredenburg, *Europhys. Lett.* **91**, 46004 (2010).
- [21] S. van der Geer, E. Vredenburg, O. Luiten, and M. de Loos, *J. Phys. B: At. Mol. Opt. Phys.* **47**, 234009 (2014).
- [22] L. Kime, A. Fioretti, Y. Bruneau, N. Porfido, F. Fuso, M. Viteau, G. Khalili, N. Šantić, A. Gloter, B. Rasser *et al.*, *Phys. Rev. A* **88**, 033424 (2013).
- [23] E. Moufarej, M. Vielle-Grosjean, G. Khalili, A. J. McCulloch, F. Robicheaux, Y. J. Picard, and D. Comparat, *Phys. Rev. A* **95**, 043409 (2017).
- [24] A. J. McCulloch, R. W. Speirs, J. Grimmel, B. M. Sparkes, D. Comparat, and R. E. Scholten, *Phys. Rev. A* **95**, 063845 (2017).
- [25] J. J. McClelland, A. V. Steele, B. Knuffman, K. A. Twedt, A. Schwarzkopf, and T. M. Wilson, *Appl. Phys. Rev.* **3**, 011302 (2016).
- [26] T. Arion and U. Hergenhahn, *J. Electron Spectrosc. Relat. Phenom.* **200**, 222 (2015).
- [27] R. Dörner, V. Mergel, O. Jagutzki, L. Spielberger, J. Ullrich, R. Moshhammer, and H. Schmidt-Böcking, *Phys. Rep.* **330**, 95 (2000).
- [28] B. D. DePaola, R. Morgenstern, and N. Andersen, *Adv. At. Mol. Opt. Phys.* **55**, 139 (2008).
- [29] C. Sahin, P. Geppert, A. Müllers, and H. Ott, *New J. Phys.* **19**, 123005 (2017).
- [30] D. A. Dahl, SIMION, <http://www.simion.com/>, Scientific Instrument Services, Inc., 1027 Old York Rd., Ringoes, NJ 08551, United States (2011).
- [31] S. B. van der Geer and M. J. de Loos, *General Particle Tracer*, [www.pulsar.nl/gpt](http://www.pulsar.nl/gpt) (2011).
- [32] R. W. Speirs, A. J. McCulloch, B. M. Sparkes, and R. E. Scholten, *Phys. Rev. A* **95**, 053408 (2017).
- [33] A. Akimov, E. Tereshchenko, S. Snigirev, A. Samokotin, A. Sokolov, N. Kolachevskii, and V. Sorokin, *J. Exp. Theor. Phys.* **109**, 359 (2009).
- [34] H. B. Bebb, *Phys. Rev.* **153**, 23 (1967).
- [35] O. Katz, Y. Bromberg, and Y. Silberberg, *Appl. Phys. Lett.* **95**, 131110 (2009).
- [36] S. H. W. Wouters, G. ten Haaf, R. P. M. J. W. Notermans, N. Debernardi, P. H. A. Mutsaers, O. J. Luiten, and E. J. D. Vredenburg, *Phys. Rev. A* **90**, 063817 (2014).
- [37] G. ten Haaf, S. Wouters, S. van der Geer, E. Vredenburg, and P. Mutsaers, *J. Appl. Phys.* **116**, 244301 (2014).